DOI:
10.1021/acs.nanolett.7b01676

Document Version
Peer reviewed version

Tracking nano-electrochemistry using individual plasmonic nanocavities

G. Di Martino,[1*] V. A. Turek, [1] A. Lombardi,[1] I. Szabó,[2] B. de Nijs, [1] A. Kuhn,[3]
E. Rosta,[2] J.J. Baumberg[1*]

[1] *NanoPhotonics Centre, Cavendish Laboratory, University of Cambridge, CB3 0HE, UK*
[2] *Department of Chemistry, King's College London, SE1 1DB, UK*
[3] *Univ. Bordeaux, CNRS 5255, Bordeaux INP, Site ENSCBP, 33607, Pessac, France*

We study in real time the optical response of individual plasmonic nanoparticles on a mirror, utilised as electrodes in an electrochemical cell when a voltage is applied. In this geometry, Au nanoparticles are separated from a bulk Au film by an ultrathin molecular spacer. The nanoscale plasmonic hotspot underneath the nanoparticles locally reveals the modified charge on the Au surface and changes in the polarizability of the molecular spacer. Dark field and Raman spectroscopy performed on the same nanoparticle, show our ability to exploit isolated plasmonic junctions to track the dynamics of nano-electrochemistry. Enhancements in Raman emission and blue-shifts at negative potential show the ability to shift electrons within the gap molecules.

KEYWORDS: Electrochemistry, plasmonics, self-assembled monolayer, dark field spectroscopy, surface enhanced Raman spectroscopy.

The plasmonic response of metal nanostructures has motivated both fundamental nano-optical investigations, as well as exploration of applications such as surface enhanced Raman spectroscopy (SERS)[1], quantum information processing[2,3], photovoltaic cells[4] and device engineering[5]. In order to actively tune plasmonic systems which can trap light of particular resonant colours, control of the local charge density as well as the surrounding dielectric environment is crucial. Electrochemical methods offer unrivalled control of surface chemistry at metal electrodes[6] and can modify the surface charge density[7–9]. The resulting interest in spectro-electrochemical tuning of the plasmon resonance of single particles has however proved puzzling. Some tuning mechanisms have been identified as chemical rather than physical in origin[7]. 'Plasmon voltammetry' on coupled Au nanoparticles has been used for sensing sulphate, acetate, and perchlorate adsorption, without yet identifying detailed mechanisms[8]. Plasmon tuning by the redox chemistry of Ag/AgCl spacers between Au nanoparticles has also been observed[10]. While such chemical transformations indeed modify the plasmons, few studies examine field-induced physical changes in the surface structural and electronic configurations. Electrochemical studies tracking Raman spectroscopy within gold gaps that sandwich a single molecular layer have

proposed that the potential-dependent Raman emission depends on molecular torsion angles[9]. Shifts in the scattering resonance of single Au nanoparticles following application of a negative bias have been attributed to an increase in the NP electron concentration (n) via electron transfer from the ITO substrate[11,12]. However this work suggests that the scattering cross-section $S_{\mathrm{scat}}(\lambda)$ is surprisingly nonlinear. We further note that in such electrochemical cells, it is crucial to reference the potential by incorporating a third electrode in-situ, which is rarely attempted[13]. Full understanding of how the nano-electrochemical environment influences such tightly-confined plasmonic resonances thus remains rudimentary.

Here we study electrodes supporting individual Au nanoparticle-on-mirror (NPoM) constructs immersed in an electrochemical solution (Figure 1a). We simultaneously investigate two fundamental light-matter interactions under changing electric potential: resonant light scattering and SERS. In the NPoM geometry, Au NPs are separated from a bulk Au film by an ultrathin molecular spacer[14–16]. This geometry provides unique possibilities to study isolated plasmonic junctions while precisely applying an oriented electrochemical potential between defined contacts, and results in high sensitivity to field-induced changes occurring in the nano-gap.

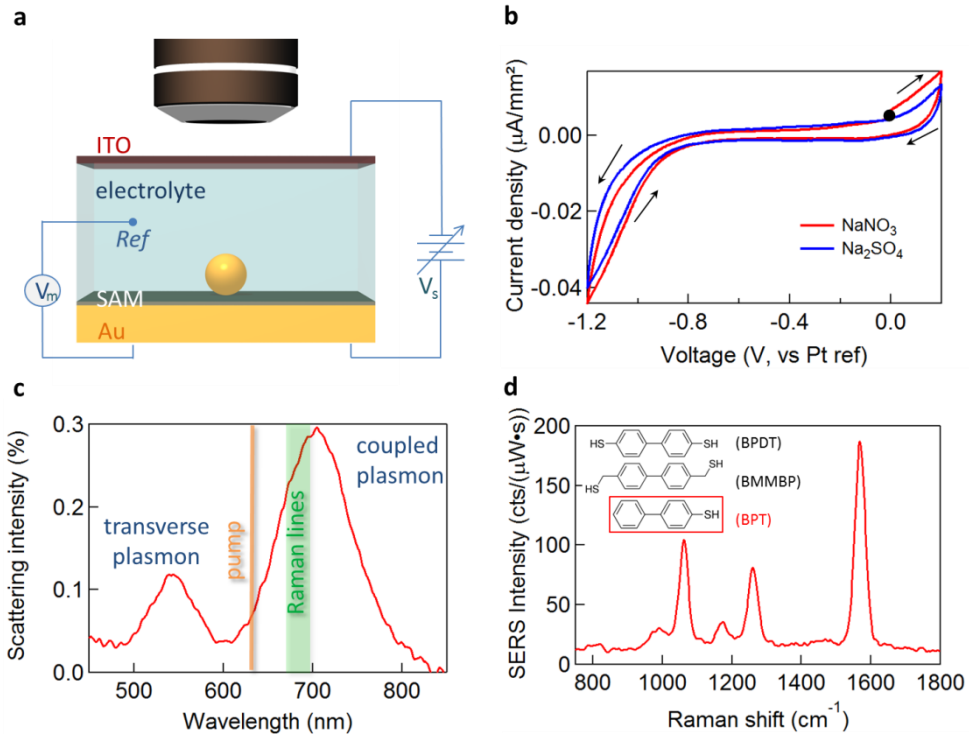

Figure 1 | Opto-electrochemistry and SERS detection. a, Optically transparent thin (sub-mm) electrochemical cell for spectroscopy of single 80 nm Au NPs on molecular layer on Au. Potential V_s applied between ITO counter electrode and Au working electrode, with Pt wire pseudo-reference electrode V_m. **b,** Typical cyclic voltammogram for biphenyl-4-thiol (BPT) on Au electrode in $NaNO_3$ and Na_2SO_4 electrolytes, starting from 0V as shown (●). **c,d,** Typical scattering spectrum (c) and surface-enhanced Raman spectrum (d) of single 80 nm Au NPoM with BPT monolayer spacer.

We drop-cast D=80 nm Au particles on top of self-assembled monolayers (SAMs) which have been previously formed on a flat Au substrate (see Methods). These samples are then immersed in a

custom-designed electrochemical cell optimized to realize both dark-field microscopy and SERS measurements on the same nanoparticle. For dark-field spectroscopy, white light irradiates single nanoparticles (average separation >5 µm) through a high numerical aperture (NA 0.8) 50× objective, with scattered light detected by a fibre-coupled cooled spectrometer (Supporting Information Figure S1). The collected spectra show a transverse plasmon mode situated around 530 nm and a coupled gap mode between 700 nm and 800 nm, depending on the thickness and conductivity of the SAM in the gap[17] (Figure 1c). To realize SERS we selectively illuminate single nanoparticles with a continuous wave (CW) laser at λ=633 nm. Initially we use biphenyl-4-thiol (BPT) spacer monolayers (Figure 1d). To study the voltage-dependent optical response of the system in real time, we apply bias using a potentiostat, with linear sweep voltammograms recorded simultaneously (Figure 1b). Various electrolytes are tested, but with no significant difference in their optical and electrical response, hence the dynamics presented below combines results from several different electrolytes.

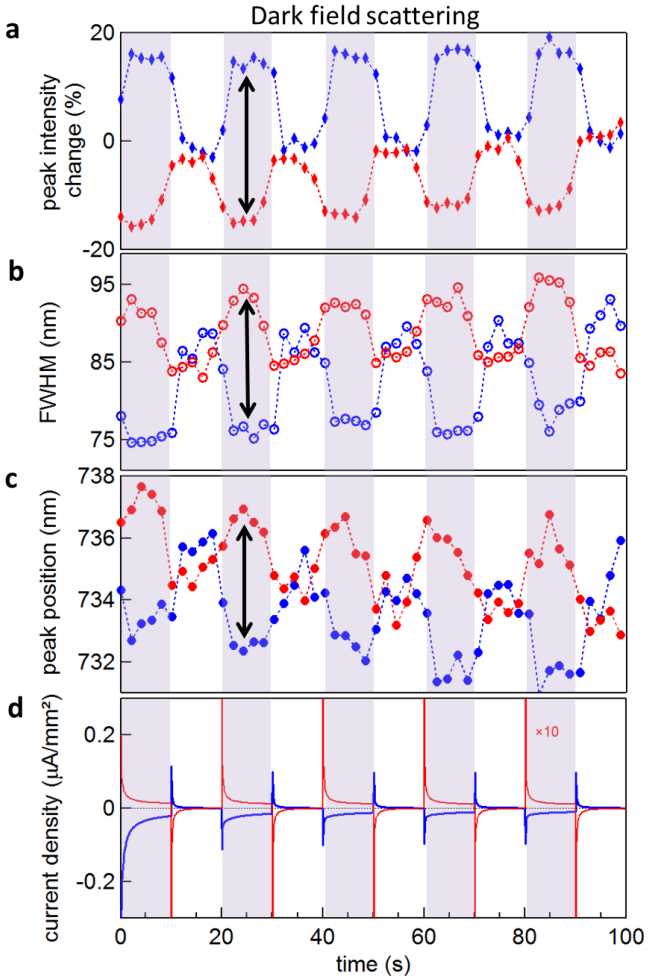

Figure 2 | Spectral dynamics under applied potential. a-c, Dynamics of dark-field scattering for NPoM with BPDT spacer in 0.1 M $MgSO_4$, revealing changes (shaded when voltage on) in (a) peak intensity, (b) resonance full width at half maximum (FWHM), and (c) spectral position of the coupled plasmon mode for negative (blue) or positive (red) voltages. **d,** Current density corresponding to optical spectra in (a-c). Square wave voltages are -1.2V ↔ 0V (blue) and +0.3V ↔ 0V (red), measured vs Pt pseudo-reference electrode.

Scattering spectra and current densities are measured while applying a square-wave potential, and show changes in the intensity, width, and spectral position of the coupled plasmon inside each single Au NPoM gap (Figure 2). The range of potentials scanned is chosen to minimise any SAM, Au, or ITO desorption or water splitting in the system[18], from -1.2V ↔ 0V (blue) and +0.3V ↔ 0V (red) measured *vs* the Pt reference electrode. Significant increases in the peak intensity, together with peak sharpening and spectral blue shifts, are observed when a negative voltage (Au substrate negatively charged) is applied (Figure 2a-c, blue). The opposite behaviour is observed (decreased amplitude, broadening, and redshifts) for positive potential (Figure 2a-c, red). These effects are fully reversible over many cycles. No evident change is observed in the transverse plasmon mode (Supporting Information Figure S2). These changes are proportional to the applied potential (Supporting Information Figures S2, S3). The same behaviour is observed for all Au NPoMs measured, although we find variations in the magnitude of their responses (Supporting Information Figs.S2-S4). We also measure NPoM electrochemical tuning with different molecular SAMs (Supporting Information Figure S3), with no significant differences observed between conducting (BPDT) or insulating (BMMBP) SAMs (Supporting Information Figure S4, refer to Figure S6 for SAMs molecular conductivity). However substantial differences are observed in the Raman response as we now discuss.

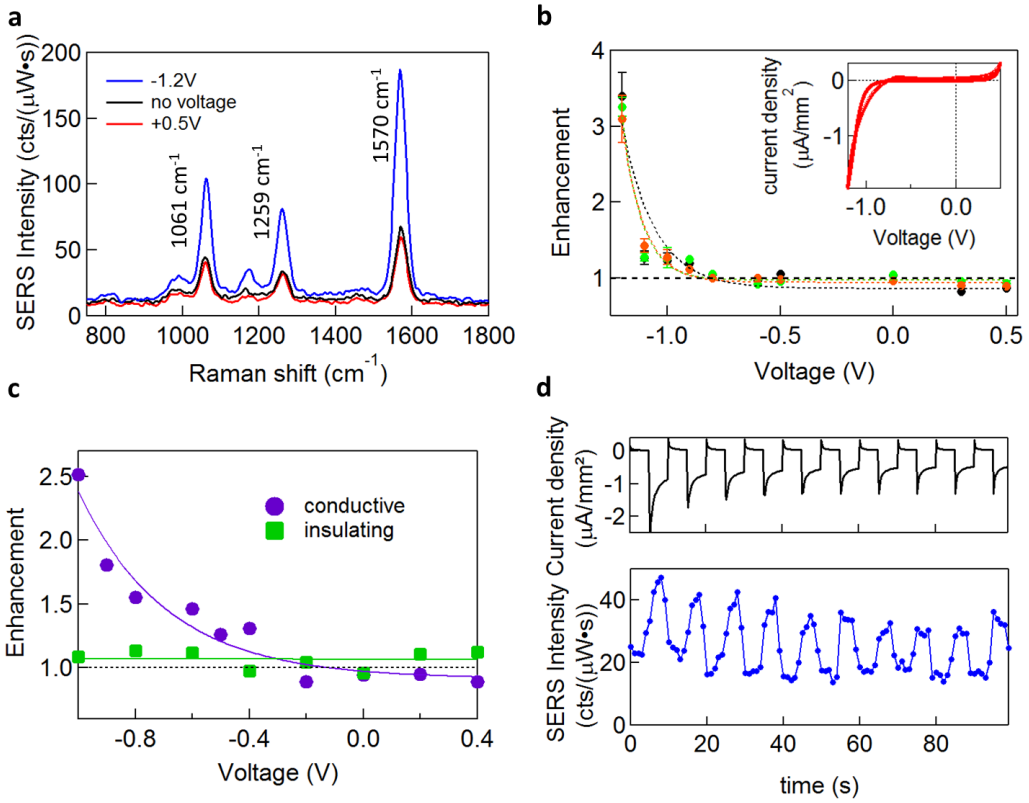

Figure 3 | SERS evolution with applied potential. a, SERS spectra of BPT in 0.1M Na_2SO_4 for negative (blue), positive (red), and no voltage (black). **b,** SERS enhancement for BPT layer given by ratio I_V/I_0 between SERS intensity with voltage (I_V) to SERS intensity when no voltage (I_0) is applied, for each vibrational line (1570 cm^{-1} in black, 1259 cm^{-1} in green, 1061 cm^{-1} in orange), and the associated cyclic voltammogram (inset). Dotted lines are fits, error bars are from standard deviation over 3 measurements on the same NP. **c,** SERS enhancement for conductive BPDT (purple) and insulating BMMBP (green) layers. Solid lines are fits. **d,** Current density (black) and corresponding SERS intensity (blue) over ten 0V ↔ -1.2V cycles, showing the reversibility of the enhancement process.

The SERS signals measured on NPoMs with a BPT spacer show strong enhancement for all vibrational lines when applying a negative bias (Figure 3a, blue). On the other hand a positive bias results in a small reduction of the SERS signals (Figure 3a, red). The size of the SERS enhancement strongly depends on the strength of the applied potential and varies for different particles, with a maximum 400% enhancement measured at the most negative potentials. This enhancement cannot be explained by the torsion of BPT molecules previously proposed[9], since the intensity of the Raman line at 1570 cm^{-1} (tangential C=C stretch in the two phenyl rings) should be more affected by torsion compared to the line at 1061cm^{-1} (C_{ring}–S stretching) while instead we find the same enhancements for different Raman peaks (Figure 3b). Interestingly, the applied potential has no effect on the SERS signals when *insulating* self-assembled molecular monolayers such as BMMBP are used as spacers (Figure 3c). These results are reproducible, having been repeatedly observed on different particles, different samples, and different electrochemical solutions (See Supporting Information). Moreover we find the process fully reversible over many cycles (Figure 3d).

As noted above, nano-plasmonic spectro-electrochemistry remains confusing. One advantage of the NPoM construct adopted here is its well-defined geometry (with observations on only ~100 molecules[17]), enabling controlled investigations to be formulated. The situation is complicated by the presence of solvent charge double layers and hydrophobic SAMs which influence high-frequency conduction within and between the gold components. Unlike nanoparticles in solution which can charge up, experiments on *dc* charge transport have shown this is not possible when the metal substrate is so close to the nanoparticles[19,20]. Such work demonstrated that electrons can be transferred between two metals across gaps with thicknesses as large as 6.5 nm,[21] at rates much faster than electron transfer between metal and dilute redox species in solution (estimates suggest up to 10^{12} times faster through a SAM than redox transfer at the metal surface[22,23]). This would evidence that the potential of the Au nanoparticle is identical to the electrode surface, preventing any account based on electric dipole modulation within the molecules in the gap that modifies the strength of the SERS signal.

As a result we explore several possible explanations, prompted by our observations. The first possibility is that the potential-driven modification of the double layer changes the local refractive index in the vicinity of the gap enough to tune the plasmons. While the modulation of refractive index in bulk salt solutions is not enough to explain the spectral shifts (Δn=0.1 would be needed in the gap to explain the shifts observed), ordering of water and double layers around, or penetration of charge into, the hydrophobic SAM might be involved. Comparing electrolytes of tetrabutyl ammonium (TBA), $MgSO_4$, and $NaNO_3$ which involve ions with larger (TBA^+) or smaller (Mg^{2+},Na^+) hydration spheres, should then give different charge penetration into the SAM producing different local refractive index changes, however no substantial differences are observed.

A second possibility is that the surface currents which drive plasmons are modulated by individual ionic charges in the solvated double layer just above the Au surface. Developing a model[24] to compare to our observations, however, gives unfeasibly large Debye lengths for the double layer as well as

matching poorly to the width of the plasmon resonance. This model would also suggest that the enhancement of SERS should be seen for insulating as well as conducting molecules, in contrast with our observations.

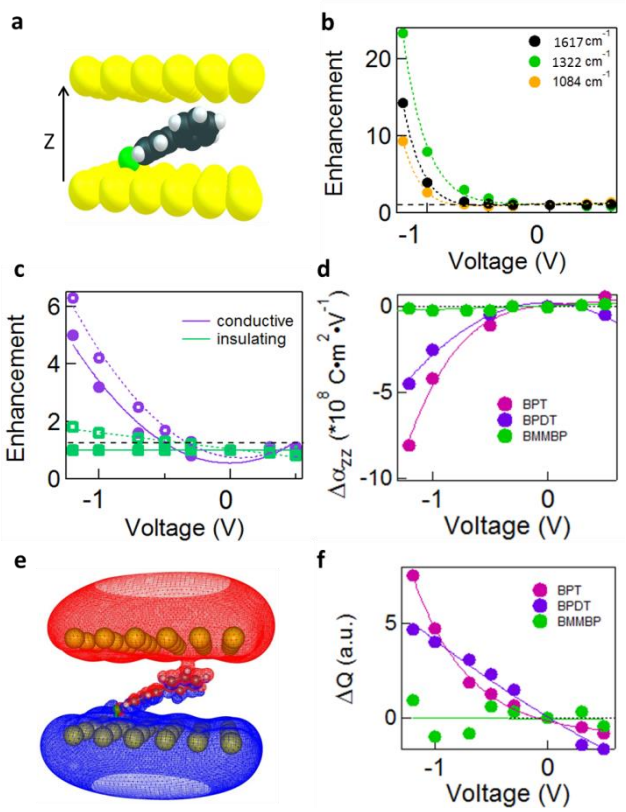

Figure 4 | DFT simulations. a, Individual spacer molecule (BPT) in SAM between Au atomic layers, field applied along z. **b-d**, Numerical simulation of SERS enhancement *vs* different applied voltages for (b) 1617 cm^{-1}, 1322 cm^{-1} and 1084 cm^{-1} Raman peaks in BPT, and (c) 1619 cm^{-1} (●) and 1088 cm^{-1} (○) in conductive BPDT (purple) and 1646 cm^{-1} (▪) and 1092 cm^{-1} (□) in insulating BMMBP (green). **d,** Polarizability element relative to $\alpha_{zz,\ 0V}$ in the direction of applied field z, for BPT, BPDT and BMMBP. **e,** Increasing (red) and decreasing (blue) electrostatic potential upon applied voltage. **f,** Charge changes on the sulphur atom *proximal to the mirror* for BPT, BPDT and BMMBP with applied voltage.

We thus explore a third possibility, which is based on a non-equilibrium potential difference appearing across the gap. To show this accounts for the SERS enhancements, we use DFT simulations which apply this potential across Au atoms surrounding individual spacer molecules (Figure 4a, see Methods). These simulations systematically reproduce the SERS enhancements experimentally observed at negative voltages (Figure 4b,c). For positive voltage the BPT is predicted to show almost no change in Raman intensity (Figure 4b). The insulating BMMBP molecule is predicted correctly to show no Raman enhancement (Figure 4c, green, as in Figure 3c).

These predictions can be understood by considering the polarizability of the molecules. From the polarizability tensor $\boldsymbol{\alpha}$, strong changes in α_{zz} are extracted when negative voltages are applied to BPT and BPDT (Figure 4d). The large applied *dc* fields (reaching 10^7 V cm^{-1}) shift the electron distribution within each molecule (Figure 4e-f), enhancing their Raman cross sections by modulating their static

electric dipoles. In particular, charge enters the molecule through the conducting S linker (Fig.4f). Insulating molecules in which electron movement is prevented show no such SERS enhancements.

This latter explanation best explains the combined observations, but opposes previous results showing no potential can be electrochemically applied across a NPoM construct. We suggest that non-equilibrium currents are responsible, as these are correlated to the observed enhancements (Figure 3d). Removing dissolved oxygen has no effect on these SERS enhancements, while the reversibility observed precludes explanations based on breakdown of the thiol-bound SAM layer. The increase in current observed for high negative potential suggests the presence of surface reactions. The likely reversible process is H^+ reduction to form H_2 gas trapped around the NPs. This would result in NP charging competing with electron tunnelling through the molecular layer, to allow a non-equilibrium and extremely large electric field to be formed between the NP and the underlying electrode. This can reorient electrons along the BPT, changing the SERS intensity as is predicted. While the substrate remains protected by the SAM, H^+ around the NP appears to slowly build up on successive CV-scans (Supporting Information Figure S5a). Increasing currents for negative voltages imply that H^+ is continuously provided by the solution. To prove this, we introduce 0.01 µM HNO_3 in 0.1 M $NaNO_3$ and verify that the onset of both the reduction current and the SERS enhancement start at lower applied potentials for lower pH electrolyte (Supporting Information Figure S5b-c). Surface reactions can thus transiently charge plasmonic structures, applying strong local fields on the nanoscale that polarise molecular interlayers, modifying their vibrational response. The gradual activation of the hydrogen evolution on successive CV-scans can also be attributed to a progressive loss of the stabilizing citrate layer coating the Au NPs. However, as the gap resistance is dominated by the hydrophobic SAM under the NPs, this should not influence the SERS dynamics[17,25].

Comparing the SERS enhancements (Fig.3c) with DFT (Fig.4c) gives potentials of ~1V, needing excess charge of $\Delta Q = CV = 28q_e$ per NP (with NP capacitance $C = 2\pi\varepsilon_0 D$). Given measured currents of 5 pA per NP, this implies a resistance of $R = V/I = 200$ GΩ, and a time constant $RC \sim 1\mu s$ (See Supporting Information for details). To sustain the non-equilibrium potential thus requires that the H^+ reduction rate exceeds 28 μs^{-1} on each NP, so that R is then the junction resistance composed of 100 molecules in parallel. This implies that the resistance of each BPT molecule is far below the quantum conductance, as previously suggested[17]. However this disagrees with [19–22].

The non-equilibrium charging of each Au NP by $\Delta Q = 28q_e$ only changes its free electron density by a fraction $\Delta Q/Q \sim 5\text{x}10^{-7}$, much too small to give the spectral shift observed, $\Delta\lambda/\lambda \sim 3\text{x}10^{-3}$ (Figure 2c). For positive voltages where no surface currents are measured, plasmon red-shifts are still obtained. The dynamics observed implies that double-layer charging is not involved, since its sharp initial current spike (Figure 2d) gives minimal rapid response in either scattering spectral shifts or SERS enhancements[1]. Instead in both cases, a slower response emerges (Figure 2a, 3d) as the local field

[1] A mismatch of one data point between the optical and electrical response is accounted for by the different integration times for the optical scattering and SERS spectra (1s) which are an order of magnitude longer than the electrical measurement (100ms).

builds up across the gap from H^+ reduction around each nanoparticle. These studies allow a much more quantitative approach to nano-electrochemistry than previously, showing the importance of non-equilibrium potential charging, and pointing to an unresolved mechanism for plasmon tuning.

In conclusion, we study the optical response of Au nanoparticles in a NPoM geometry, separated from bulk Au electrodes by an ultrathin hydrophobic molecular spacer in an electrochemical solution. We measure real-time scattering spectra and SERS signals on individual Au NPs when a voltage is applied across the electrochemical cell, impossible to achieve in colloidal nanoparticle suspensions. This field influences the charge double layer and encapsulated molecules within the tightly-confined plasmonic hotspot underneath the NPs. We suggest several mechanisms that can modulate the plasmonic resonance and SERS enhancements, identifying the displacement of electrons within each spacer molecule. Our results show the capability to track nano-electrochemistry using individual plasmonic nanocavities, and illustrate the complexity of the composite nano-construct electrode. Such work is vital to provide an improved understanding of surface chemistry, crucial for catalysis, as well as a host of photo-electrochemical applications.

METHODS

Sample preparation. Gold substrates are prepared by evaporating a 5 nm chromium adhesion layer and 70 nm gold layer on a silicon (100) wafer (Si-Mat, Germany) at a rate of 0.5 Å/s. Self-assembled monolayers of biphenyl-4-thiol (BPT), biphenyl-4,4'-dithiol(BPDT), 4-mercaptobenzoic acid (MBA), and 4,4'-bis(mercaptomethyl)biphenyl (BMMBP) (Sigma-Aldrich, 97%, 95%, 99% and 97%, respectively) are formed by submerging the substrates into a 1 mM solution in water-free ethanol (Sigma-Aldrich, reagent grade, anhydrous) for 12 h. The samples are subsequently thoroughly rinsed with ethanol and blown dry. Citrate capped gold nanoparticles (BBI Solutions, UK) are deposited by drop casting from the as-received solution. The deposition time is adjusted in order to obtain the desired nanoparticle coverage. The samples are rinsed with Milli-Q water in order to remove any salt residues.

Electrochemical cell assembly. The Au substrate (working electrode) is sandwiched between an 8-12Ω indium-tin-oxide (ITO)-coated glass cover slip (counter electrode) and a glass microscope coverslip. The electrochemical cell is assembled so that half of the substrate is immersed in liquid while the other half is dry and electrically contacted with copper tape. A Pt wire (pseudo-reference electrode, 0.5 mm diameter) is inserted into the electrochemical cell and immersed in the aqueous solution. Different 0.1M solutions are tested ($NaNO_3$, Na_2SO_4, $MgSO_4$ and TBA) with no significant difference in the optical response. The potentiostat is an Ivium Technologies (CompactStat.h).

Dark-Field spectroscopy. Optical dark-field images are recorded on a custom Olympus GX51 inverted microscope. Samples are illuminated with a focused white light source (halogen lamp). The scattered

light is collected through a 50× dark-field objective (LMPLFLN-BD, NA 0.8) and analysed with a fiber-coupled (50 μm optical fiber) Ocean Optics QE65000 cooled spectrometer. We use a standard diffuser as a reference to normalize white light scattering.

SERS analysis. SERS experiments are performed on the same modified Olympus GX51 inverted microscope used for dark-field spectroscopy. A monochromatic 633 nm HeNe laser beam is focused on the sample using a 50× objective (NA 0.8). Raman scattering is collected through the center of the objective and analysed with a Shamrock SR-303i spectrometer (600 l/mm 650nm blazed grating) coupled with an EMCCD camera cooled to −85°C. Rayleigh scattering is filtered out with a long pass 633nm filter. The system is calibrated using a silicon substrate as a reference. Spectral acquisitions are taken using an integration time of 1 s and the laser power on the sample is 30μW, with dark counts of the EMCCD subtracted. The lack of significant background, which originates from the electronic continuum in the metal[26], is a consequence of the high field localization within the molecular gap layer.

Numerical simulations. Full quantum mechanical computations were performed to reveal the optical properties of BPT-Au, BPDT-Au, BMMBP-Au model systems, which consists of single BPT, BPDT, and BMMBP molecules confined between two parallel gold monolayers. Gas phase geometry optimisations were performed using density functional theory at the B3LYP level of theory in combination with the LANL2DZ basis set. Frequency computations were performed at the same level of theory to obtain the Raman frequencies and activities. Both geometry optimisations and frequency computations were performed without symmetry, i.e. in the input orientation. In all calculations the gold atoms were frozen and the distance between gold layers was fixed at 9.25, 10.05, and 14.85 Å for BPT, BPDT, and BMMBP, respectively. To simulate the effect of applied voltage, an electric dipole field was applied perpendicular to the gold layers by invoking the Gaussian 09 Field code. The geometries of BPT, BPDT and BMMBP were optimised at each electric dipole field. The charge distribution is obtained using the Natural Bond Analysis (NBO) package[27,28]. Computational simulations were carried out with the Gaussian 09 program package.

Acknowledgements

We acknowledge financial support from EPSRC grant EP/G060649/1, EP/L027151/1, EP/G037221/1, EP/N020669/1, EPSRC NanoDTC, and ERC grant LINASS 320503.

Author Contributions

Experiments were performed by G.D., A.L. and V.A.T., with support for the chemical nanoassembly and sample preparation from V.A.T. Simulations were performed by E.R., I.S. The data analysis was

performed by G.D., with support from A.K. for the electrochemical understanding. G.D., V.A.T. and J.J.B. designed the experiments. All authors contributed to the manuscript.

Corresponding Authors

*E-mail: gd392@cam.ac.uk, jjb12@cam.ac.uk

Supporting Information

Supporting Information Available: detailed optical setup; additional spectral dynamics for various applied voltages, spacers and solutions; analytical model derivation. This material is available free of charge via the Internet at http://pubs.acs.org.

Notes

The authors declare no competing financial interest.

References

(1) Kneipp, K.; Wang, Y.; Kneipp, H.; Perelman, L. T.; Itzkan, I.; Dasari, R. R.; Feld, M. S. *Phys. Rev. Lett.* **1997**, *78*, 1667–1670.
(2) Di Martino, G.; Sonnefraud, Y.; Tame, M. S.; Kéna-Cohen, S.; Dieleman, F.; Özdemir, Ş. K.; Kim, M. S.; Maier, S. A. *Phys. Rev. Appl.* **2014**, *1*, 034004.
(3) Tame, M. S.; McEnery, K. R.; Özdemir, Ş. K.; Lee, J.; Maier, S. A.; Kim, M. S. *Nat. Phys.* **2013**, *9*, 329–340.
(4) Atwater, H. A.; Polman, A. *Nat. Mater.* **2010**, *9*, 205–213.
(5) Di Martino, G.; Tappertzhofen, S.; Hofmann, S.; Baumberg, J. *Small* **2016**, *12*, 1334–1341.
(6) Kolb, D. M. *Surf. Sci.* **2002**, *500*, 722–740.
(7) Byers, C. P.; Hoener, B. S.; Chang, W.-S.; Yorulmaz, M.; Link, S.; Landes, C. F. *J. Phys. Chem. B* **2014**, *118*, 14047–14055.
(8) Byers, C. P.; Hoener, B. S.; Chang, W.-S.; Link, S.; Landes, C. F. *Nano Lett.* **2016**, *16*, 2314–2321.
(9) Cui, L.; Liu, B.; Vonlanthen, D.; Mayor, M.; Fu, Y.; Li, J.-F.; Wandlowski, T. *J. Am. Chem. Soc.* **2011**, *133*, 7332–7335.
(10) Byers, C. P.; Zhang, H.; Swearer, D. F.; Yorulmaz, M.; Hoener, B. S.; Huang, D.; Hoggard, A.; Chang, W.-S.; Mulvaney, P.; Ringe, E.; Halas, N. J.; Nordlander, P.; Link, S.; Landes, C. F. *Sci. Adv.* **2015**, *1*, e1500988.
(11) Collins, S. S. E.; Wei, X.; McKenzie, T. G.; Funston, A. M.; Mulvaney, P. *Nano Lett.* **2016**, *16*, 6863–6869.
(12) Brown, A. M.; Sheldon, M. T.; Atwater, H. A. *ACS Photonics* **2015**, *2*, 459–464.
(13) Bard, Allen J.; Faulkner, Larry R. *Electrochemical Methods: Fundamentals and Applications.*, 2nd ed.; Wiley, 2000.

(14) Mubeen, S.; Zhang, S.; Kim, N.; Lee, S.; Krämer, S.; Xu, H.; Moskovits, M. *Nano Lett.* **2012**, *12*, 2088–2094.
(15) Daniels, J. K.; Chumanov, G. *J. Phys. Chem. B* **2005**, *109*, 17936–17942.
(16) Mertens, J.; Eiden, A. L.; Sigle, D. O.; Huang, F.; Lombardo, A.; Sun, Z.; Sundaram, R. S.; Colli, A.; Tserkezis, C.; Aizpurua, J.; Milana, S.; Ferrari, A. C.; Baumberg, J. J. *Nano Lett.* **2013**, *13*, 5033–5038.
(17) Benz, F.; Tserkezis, C.; Herrmann, L. O.; de Nijs, B.; Sanders, A.; Sigle, D. O.; Pukenas, L.; Evans, S. D.; Aizpurua, J.; Baumberg, J. J. *Nano Lett.* **2015**, *15*, 669–674.
(18) Thom, I.; Buck, M. *Surf. Sci.* **2005**, *581*, 33–46.
(19) Zhao, J.; Wasem, M.; Bradbury, C. R.; Fermín, D. J. *J. Phys. Chem. C* **2008**, *112*, 7284–7289.
(20) Bradbury, C. R.; Zhao, J.; Fermín, D. J. *J. Phys. Chem. C* **2008**, *112*, 10153–10160.
(21) Zhao, J.; Bradbury, C. R.; Fermín, D. J. *J. Phys. Chem. C* **2008**, *112*, 6832–6841.
(22) Chazalviel, J.-N.; Allongue, P. *J. Am. Chem. Soc.* **2011**, *133*, 762–764.
(23) Barfidokht, A.; Ciampi, S.; Luais, E.; Darwish, N.; Gooding, J. J. *Anal. Chem.* **2013**, *85*, 1073–1080.
(24) Di Martino, G.; Turek, V.; Tserkezis, C.; Lombardi, A.; Kuhn, A.; J. Baumberg, J. *Faraday Discuss.* **2017**.
(25) Benz, F.; Nijs, B. de; Tserkezis, C.; Chikkaraddy, R.; Sigle, D. O.; Pukenas, L.; Evans, S. D.; Aizpurua, J.; Baumberg, J. J. *Opt. Express* **2015**, *23*, 33255–33269.
(26) Mahajan, S.; Cole, R. M.; Speed, J. D.; Pelfrey, S. H.; Russell, A. E.; Bartlett, P. N.; Barnett, S. M.; Baumberg, J. J. *J. Phys. Chem. C* **2010**, *114*, 7242–7250.
(27) Reed, A. E.; Curtiss, L. A.; Weinhold, F. *Chem. Rev.* **1988**, *88*, 899–926.
(28) Foster, J. P.; Weinhold, F. *J. Am. Chem. Soc.* **1980**, *102*, 7211–7218.

Table of Contents